Metals and Materials International (2023) 29:59–70
https://doi.org/10.1007/s12540-022-01205-9

Determining the Optimum Process Parameters of Selective Laser Melting via Particle Swarm Optimization Based on the Response Surface Method

Fahri Murat[1] · İrfan Kaymaz[1] · Abdullah Tahir Şensoy[2] · İsmail H. Korkmaz[1]

Received: 10 January 2022 / Accepted: 17 March 2022 / Published online: 3 June 2022

Abstract
Manufacturing high-quality and desired products from additive manufacturing necessitate careful adjustment of the process parameters. Various methods can be utilised to determine optimum process parameters, such as the Taguchi method, Design of Experiments (DoE). Rather than evaluating limited information obtained from statistical analysis of the experiments, optimisation methods can help find the best possible combination for the process parameters. Therefore, an optimisation approach based on Particle Swarm Optimization (PSO) was utilised to find the optimum process parameters. The most important process parameters of Selective Laser Melting (SLM) such as laser power, layer thickness, scan speed, and build orientation were selected as input parameters, and their effects on the tensile properties of the manufactured part were investigated to find out the optimal operating conditions for the SLM process. Since there is not any explicit mathematical expression relating these process parameters to the tensile strength, the Response Surface Method (RSM) was used to obtain a meta-model so that it can be used as an objective function in the optimisation formulation. This approach enabled us to predict the optimum process parameters to maximise the tensile strength without conducting an excessive number of experiments. Moreover, the mathematical model can also predict tensile strength corresponding to the parameter values that are not tested according to the DoE chosen for such studies. Furthermore, it was also shown that the PSO outperforms the Genetic Algorithm (GA), which is widely employed to find out the optimum process parameters, in terms of less number of iteration.

Keywords Powder bed fusion · Ti6Al4V · Central composite design · Particle swarm optimization · Genetic algorithms

1 Introduction

Ti6Al4V alloy is a widely used material especially for lightweight construction and load-bearing implants due to its corrosion resistance, high strength/density ratio and excellent biocompatibility [1, 2]. However, manufacturing components from bulk Ti6Al4V using traditional technologies requires high-quality cutting tools and process conditions due to its high strength and toughness. Extra care must be taken since titanium alloy can easily react with oxygen, nitrogen, hydrogen and carbon in thermal processes [3]. In this respect, Selective Laser Melting (SLM) as an Additive Manufacturing (AM) technique has been of great interest in recent years due to its superior benefits such as ease of manufacturability of the complex-shaped parts, producing lightweight structures using topology optimization [4, 5]. On the other hand, the quality of additive manufactured parts depends mainly on the process parameters of the SLM process. Therefore, a great number of researches have been

✉ Fahri Murat
fahri.murat@erzurum.edu.tr

İrfan Kaymaz
irfan.kaymaz@erzurum.edu.tr

Abdullah Tahir Şensoy
tahir.sensoy@samsun.edu.tr

İsmail H. Korkmaz
ismail.korkmaz@erzurum.edu.tr

[1] Department of Mechanical Engineering, Faculty of Engineering and Architecture, Erzurum Technical University, 25050 Erzurum, Turkey

[2] Department of Biomedical Engineering, Faculty of Engineering, Samsun University, 55060 Samsun, Turkey

conducted to determine these process parameters and their effects on the parts produced. For example, Olaf et al. [6] estimated that more than 130 parameters could affect the SLM process, of which about 13 are crucial to the properties of the manufactured parts.

Regarding the SLM parameters affecting Ti6Al4V parts, it was reported that high energy density, for which laser power and scan speed greatly influence, causes over-melting, thus leading to defects formation [6, 7]. To reduce the variation in the mechanical properties of Ti6Al4V specimens with almost similar relative density, Abotaleb et al. [8] considered three parameters, namely laser power, layer thickness and hatch distance. They have shown that adjusting the value of these three parameters result in maximum relative density and elongation-to-failure. Simonelli et al. [9] studied the effect of the three build orientations on the tensile properties of Ti6Al4V parts produced using SLM. It was found that the build orientation affects both the tensile properties and the ductility of the Ti6Al4V samples. Therefore, the process parameters, including laser power, layer thickness, scan speed and build orientation, are considered the most important parameters for SLM produced Ti6Al4V alloys [5, 9]. Although these researches indicate the importance of selecting appropriate parameters and their values, it is not easy for engineers to determine the optimal values for the process parameters [10]. Therefore, choosing the best possible combination of the process parameters becomes crucial to obtain high-quality products.

Researchers have focused on determining the optimal process parameters using different approaches [10]. In this regard, there are mainly two approaches that can be used to determine the optimum process parameters. One approach is a process map by which process windows are used to guarantee certain types of part properties [6, 11]. Although the process maps can provide information to select the possible process parameters, it is time-consuming since it is based on a trial-and-error approach. Thus, more mathematically sound approaches have been recently applied based on the design of the experiments and heuristic optimisation methods. For instance, Gong et al. [7] utilised the Taguchi experiment to determine the effect of the processes parameters on the porosity of Ti–6Al–4 V samples. The central composite design (CCD) was used to find the optimum values for scanning speed and laser power [12]. Li et al. [14] used the Response Surface Method (RSM) to determine the optimal combination of SLM parameters to improve the surface roughness quality of Ti6Al4V components. Rather than evaluating limited information obtained from statistical analysis of the experiments, optimisation methods can help find the best possible combination for the process parameters. In this regard, Ma et al. [14] utilised the non-dominated sorting genetic algorithm II (NSGA-II) to find the optimum values of the three process parameters of scanning speed, gap distance, and layer thickness. Arısoy et al. [15] adopted the genetic algorithm (GA) to optimise the microstructure properties of the nickel alloy. More recently, Li et al. [11] developed an ensemble of the meta-models combining three meta-modeling techniques to find the optimum value of the process parameters by solving a multi-objective optimisation problem using NSGA-II. Ngyuen et al. [16] adopted a supervised deep neural network to optimise four SLM process parameters; laser power, laser scanning velocity, hatch distance, and layer thickness for a printed product to obtain a required density.

Compared to other heuristic search algorithms like GA, which are widely used to determine the optimum process parameters of AM, particle swarm optimization (PSO) is simple to implement and slightly performs better in terms of the number of iterations required to reach an optimum solution [17, 18]. Therefore, a comparison between PSO and GA has been regarding both efficiency and accuracy of the optimum results.

There are quite a few studies that use PSO to determine optimum process parameters of AM. For instance, Qin et al. [19] proposed a deep learning-driven particle swarm optimization (DLD-PSO) method to determine the optimum parameters for AM energy utilization.Shirmohammadi et al. developed an approach consisting of a hybrid artificial neural network (ANN) and PSO algorithm to optimise the input parameters of the fused deposition modeling (FDM) printing process to obtain minimum surface roughness.

The response surface method (RSM) can be effectively used to create a relationship between input and output variables of AM since it requires fewer experiments than ANN as well as using well-design design of experiments (DoE). Negi et al. [20] have investigated how the parameters such as bed temperature, laser power, scan speed, hatch distance, hatch length influence the mechanical properties of the end product by constructing a second-degree polynomial function using the RSM. The effect of each parameter on the surface roughness were evaluated considering the coefficients in the meta-model. Although the optimum values for the parameters were given by carrying out process optimisation, which optimisation algorithm was used is not specified in the paper. Read et al. [21] investigated the influence of SLM process parameters for fabricating AlSi10Mg using the RSM method, and the optimum process parameters were found using this meta-model in GA. To our knowledge, there is not any study in literature in which PSO and the RSM have been combined to find optimum process parameters yielding the maximum tensile strength of parts produced from SLM.

Therefore, to maximise the tensile strength, this study aims to find the optimum values of the most important process parameters, namely laser power, scan speed, layer thickness, and build orientation. For this purpose, the CCD was chosen as a DoE method, and the samples were

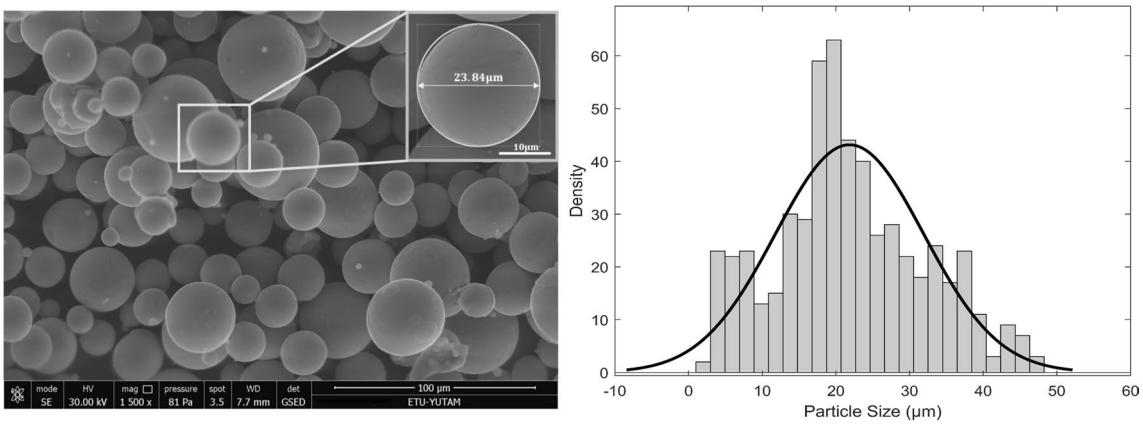

Fig. 1 SEM images and probability density distribution for the measured Ti6Al4V powders

manufactured according using Concept Laser (MLab Cusing 100R). Then, the tensile tests were conducted with Instron-5982 electromechanical static tester. The RSM based on the DoE was used as a mathematical modelling technique to obtain an explicit meta-model for the tensile strength. Thus, the mathematical model was used to determine the best possible manufacturing parameters by employing both the PSO and GA. Furthermore, a validation test was also conducted for the sample produced using the optimum process parameters obtained from the PSO.

2 Materials and Methods

2.1 Materials

One of the crucial factors affecting the layer thickness in SLM is the variation of the powder size By choosing the layer thickness in the range of 30–50 µm, the amount of powder dragged off the table by the spreading mechanism can be reduced. Thus, powders can be distributed more homogeneously on the manufacturing table, and the production can be accelerated due to higher layer thickness. Therefore, the particle size and chemical composition need to be determined first.

The images of the powder particles taken from Scanning Electron Microscope (SEM) were evaluated using IC Measure (The Imaging Source Europe GmbH, Germany) software. Each powder particle's diameter values were obtained by measuring all the particles from 10 images taken randomly from Ti6Al4V alloy powder. The probability distribution function represented the diameter values of 554 particles obtained (Fig. 1).

Based on the measurement, the powder particles' average diameter and standard deviation were calculated as 21.8534 µm and 10.0902 µm, respectively. The maximum powder particle diameter value was 48.16 µm, and the smallest particle diameter was 1.36 µm.

Table 1 Chemical composition of the Ti6Al4V powder alloy

Element	Weight%	Atomic%	Error%
Al	5.91	10.07	10.62
Ti	87.85	84.30	1.25
V	6.24	5.63	5.99

The chemical composition of Ti6Al4V directly affects the mechanical properties of parts produced by the SLM method. Therefore, the chemical composition analysis was carried out using the Energy-Dispersive Spectroscopy (EDS) method using SEM, and the results are presented in Table 1.

2.2 Experimental Method

The experiments were designed using the CCD, one of the most common methods used to generate the input for the RSM due to the rotatability and orthogonality of the designs developed. Thus, it ensures a reasonably consistent and stable variance as well as having continuous accuracy for the estimation [22]. This design model consists of 2^k factorial trials (including k factor number) whose levels are coded as -1 to $+1$. It includes n number of centre points and 2k axis points at a distance α from the centre point; thus, the number of experiments to be performed becomes $2^k + 2k + n$. The upper and lower limits of the parameters are given in Table 2. The values in the table were determined by taking into account the mean and standard deviation of the manufacturing parameters given in the literature. The powder spreader mechanism provides a powder feed of 1.5 g/s, which indicates the amount of powder used for a single layer during the spreading process with a feed rate of 70 mm/s. The hatch distance was kept constant at 0.07 mm.

Table 2 Selected process parameters and their levels

Factors	Symbol	Levels		
		− 1	0	1
Laser power [W]	*A*	80	90	100
Layer thickness [µm]	*B*	30	40	50
Scan speed [mm/s]	*C*	500	750	1250
Build orientation (Degree)	*D*	0	45	90

The tensile test samples were prepared according to the ASTM E8 standard [23]. The circular cross-section samples were used on both axes to find the optimum value of the build orientation parameter, as given in Fig. 2.

The support structures were designed to be easily removed from the table after production and have optimum heat conduction through the supports [24]. The cross-section of the samples is cylindrical, and it is 3 mm in length, 0.2 mm in diameter, and 0.1 mm in diameter at the points that contact the part and the table.

The test samples were manufactured using the Concept Laser (MLab Cusing 100R) machine with the SLM in an Argon gas atmosphere. After the production, the support structures were cleaned not to damage the gauge length. The samples were classified as given in Table 3.

The static tensile testing was carried out using Instron-5982 electromechanical static tester. The samples were tested at a constant deformation rate of 2 mm/min. As a result of the experiments, force-elongation data were obtained, and the diameter value and stress-strain properties of the sample were determined.

2.3 Particle Swarm Optimization

The concept of Particle Swarm Optimization (PSO) is based on iteratively updating the candidate swarm members to reach the optimum solution [25]. In this concept, every possible solution is considered as a swarm member. Each swarm member is called a particle (i) whose velocity (v_i) and position (x_i) differ from each other. Each particle's position and velocity are updated in the next iteration according to the comparison between the fitness results of the candidate points. Velocity and position of the particles can be represented for a D-dimensional vector space as follows;

$$x_i = \left(x_{i1}, x_{i2}, \ldots, x_{iD}\right) \tag{1}$$

$$v_i = (v_{i1}, v_{i2}, \ldots, v_{iD}) \tag{2}$$

The velocity and position of the particles are updated according to the following equations;

$$x_i(t+1) = x_i(t) + v_i(t+1) \tag{3}$$

$$v_i(t+1) = wv_i(t) + R_1c_1\left(P_i - x_i(t)\right) + R_2c_2\left(P_g - x_i(t)\right) \tag{4}$$

where R_1 and R_2 are two random values between 0 and 1; w is the inertia coefficient; c_1, c_2 are the individual and social acceleration parameters, respectively. In Eq. 4, which is illustrated in Fig. 3, P_i and P_g denote the best individual position ever, and the best position between all the swarm members in the population, respectively.

As seen in Fig. 3, $x_i(t)$ denotes the position of the particle, while the vector of $v_i(t)$ represents the direction and velocity of the particle that moves. $P_i(t)$ is the best value of particle i. $P_g(t)$ is the global best of the swarm. Since the particles are not alone and interacting, thus learning from each other, each particle improves its position as well as its velocity repeatedly by Eqs. 3 and 4, respectively. If the figure is carefully examined, it can be seen that the velocity of the particle for the following iteration ($v_i(t+1)$) can be found by adding three vectors. First-term is a proportion of $v_i(t)$, and it

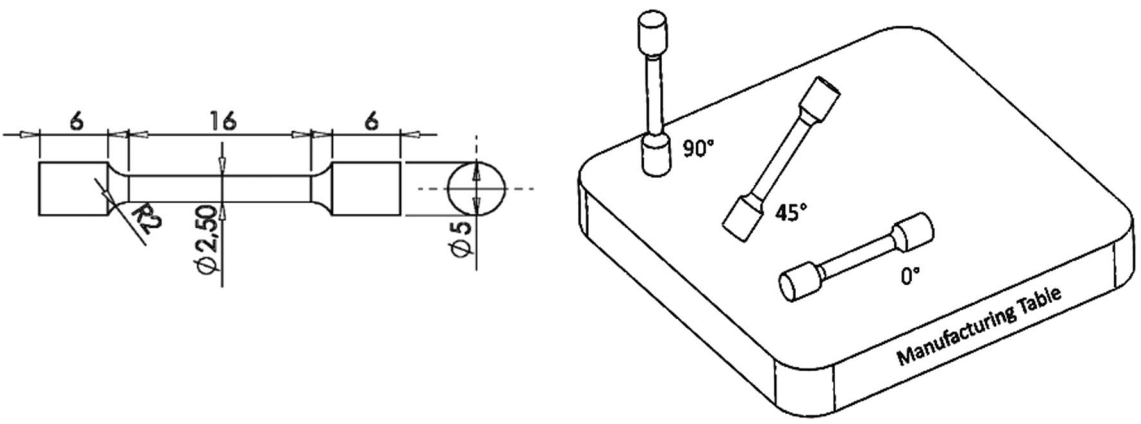

Fig. 2 Dimensional properties of the sample produced for the experimental study and sample positioning arrangement on the manufacturing table

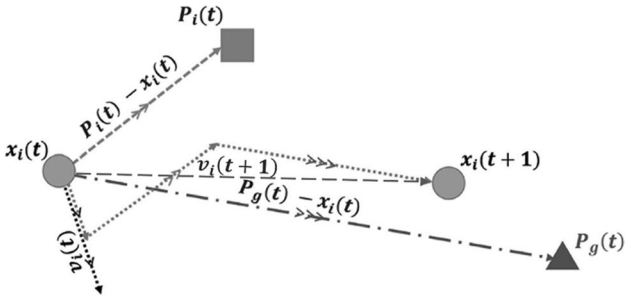

Fig. 3 Illustration of PSO [26]

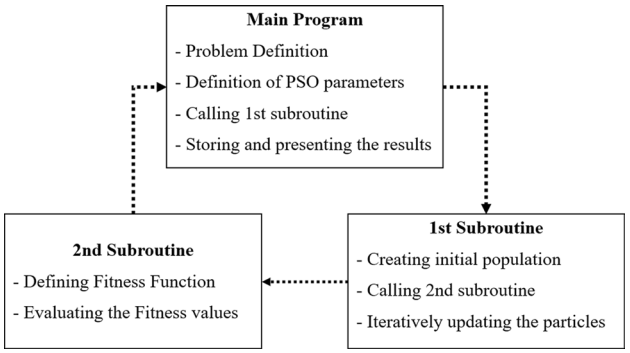

Fig. 4 Flowchart of the PSO process coded in MATLAB

can be calculated by multiplying $v_i(t)$ with the coefficient of inertia(w). The second and third terms can be calculated by multiplying the vectors of "$P_i - x_i(t)$" and "$P_g - x_i(t)$" with R_1c_1 and R_2c_2, respectively. By using the velocity of the i'th particle for the following iteration "$(v_i(t+1)$", the next position of the i'th particle is determined. This iterative process continues until the stopping criteria are satisfied.

Using the PSO concept briefly given above, the MATLAB (R2019b, The MathWorks Inc., Natick, Massachusetts) codes were developed to optimize the process parameters of AM. Three programs were written and linked to each other. The master program controls the other two subroutines and stores the results (Fig. 4).

3 Results

3.1 Tensile test results

The tensile tests based on the CCD were conducted, and the results are given in Table 3. In the CCD method, cube points, centre points in the cube, axial points, and centre points in the axial were selected as 16, 4, 8 and 2, respectively. Since there are four independent variables, 30 design points were created. The samples were named with the letter "S" and the experiment number and classified as "laser power-layer thickness-scan speed-orientation angle" in parentheses (e.g. S1.1(100-30-1250-90)). It should be noted that the experiments from S6.1(90-40-875-45) to S6.6(90-40-875-45) in Table 3 indicate the central runs at the CCD.

Some experimental results were far lower than the mean value of the tests conducted. These values are considered outliers, which were determined considering the median value of the experiment results. Thus, the experiments denoted as S2.1*(100-50-1250-90), S3.2*(100-50-500-0) and S12.1*(80-50-500-90) were not taken into account during the formation of the mathematical models.

The stress-strain curves obtained from the tensile tests for some of the samples are graphically shown in Fig. 5. Each curve in Fig. 5 was obtained, taking the average value of the three experiments conducted at the same level of the parameters. Then, the samples manufactured with different process parameters were investigated in terms of their mechanical behaviour.

The laser parameters in the experiments vary, yielding a different cooling rate of the melt pool, energy density and pore formation [25]. This results in different mechanical properties of the samples produced from the same material (Ti6Al4V), as seen in Fig. 5.

3.2 Mathematical modelling

The RSM was used to create a mathematical model by which the tensile strength value was estimated this study. In this regard, a full-quadratic model given in Eq. 5 was first selected:

$$y = \beta_0 + \sum_{i=1}^{k} \beta_i X_i + \sum_{i=1}^{k} \sum_{j>i}^{k} \beta_{ij} X_i X_j + \sum_{i=1}^{k} \beta_{ii} X_i^2 + \epsilon \quad (5)$$

where y is the corresponding response, which is the tensile strength in this study, β_0 denotes the constant coefficient, β_i, β_{ij} and β_{ii} are the coefficients for linear, interaction and quadratic effects, respectively. Table 4 presents the ANOVA results for the full quadratic response surface model for the tensile strength.

When the results given in Table 4 are examined, it can be said that the model fits well to the experimental data since the p-value of lack-of-fit in the RSM is larger than 0.05 (non-significant). All other terms in the model were evaluated at the confidence level of 95%. The terms with a larger P-value than 0.05 were remarked as non-significant. Some P-values shown as "0.000" in Table 4 means that the P-values of these sources are extremely small ($P < 0.001$), indicating that the terms are highly significant.

As goodness of fit criteria, the coefficient of determination (R^2), Adjusted-R^2 and Predicted-R^2 were determined as 0.984, 0.965 and 0.883, respectively. It is well known that terms reduction may improve the model if many insignificant

Table 3 Design of Experiment based on CCD and experimental results

Manufacturing No	Experiments No	Input parameters				Output parameter
		Laser power [W] (*A*)	Layer thickness [μm] (*B*)	Scan speed [mm/s] (*C*)	Orientation angle [°] (*D*)	Tensile strength [MPa]
1	1.1	100	30	1250	90	1154.12
	1.2	100	30	1250	0	1045.58
2	2.1*	100	50	1250	90	717.43
	2.2	100	50	1250	0	859.44
3	3.1	100	50	500	90	1247.13
	3.2*	100	50	500	0	970.66
4	4.1	100	30	500	90	1108.60
	4.2	100	30	500	0	1203.35
5	5.1	100	40	875	45	1278.50
6	6.1	90	40	875	45	1239.81
	6.2	90	40	875	45	1239.83
	6.3	90	40	875	45	1225.48
	6.4	90	40	875	45	1223.54
	6.5	90	40	875	45	1164.44
	6.6	90	40	875	45	1218.62
	6.7	90	40	875	90	1219.71
	6.8	90	40	875	0	1259.38
7	7.1	90	30	875	45	1256.97
8	8.1	90	40	1250	45	850.85
9	9.1	90	40	500	45	1251.36
10	10.1	90	50	875	45	948.71
11	11.1	80	30	500	90	1231.10
	11.2	80	30	500	0	1244.85
12	12.1*	80	50	500	90	1094.23
	12.2	80	50	500	0	1087.68
13	13.1	80	50	1250	90	282.53
	13.2	80	50	1250	0	391.27
14	14.1	80	30	1250	90	865.93
	14.2	80	30	1250	0	840.50
15	15.1	80	40	875	45	969.18

*Outliers (Determined by the standard deviation of each set)

model terms exist. R^2 and Adjusted-R^2 values are both in an acceptable range. However, the model has been improved by removing non-significant terms (except main term). The reduced quadratic response surface model was obtained as given in Eq. (6).

$$\begin{aligned} y =& 2276 - 34.16A \\ &+ 19.1B + 0.091C - 0.186D - 0.834B^2 \\ &- 0.000961C^2 + 0.641AB + 0.02238AC \\ &- 0.02394BC \end{aligned} \tag{6}$$

Thus, R^2, Adjusted-R^2 and Predicted-R^2 for the model given in Eq. 6 were obtained as 0.972,0.958 and 0.925, respectively. The removal of non-significant terms improved the Predicted-R^2value. Its value of 0.94 for the reduced quadratic model is in reasonable agreement with the Adjusted-R^2 of 0.96 since the difference is less than 20% [27]. The optimisation problem is defined as in Eq. (7) to determine the optimum process parameters that maximise the tensile strength.

$$\max F_T = f(A, B, C, D) \tag{7}$$

$$s.t.$$

$$100 \geq A \geq 80$$

$$50 \geq B \geq 30$$

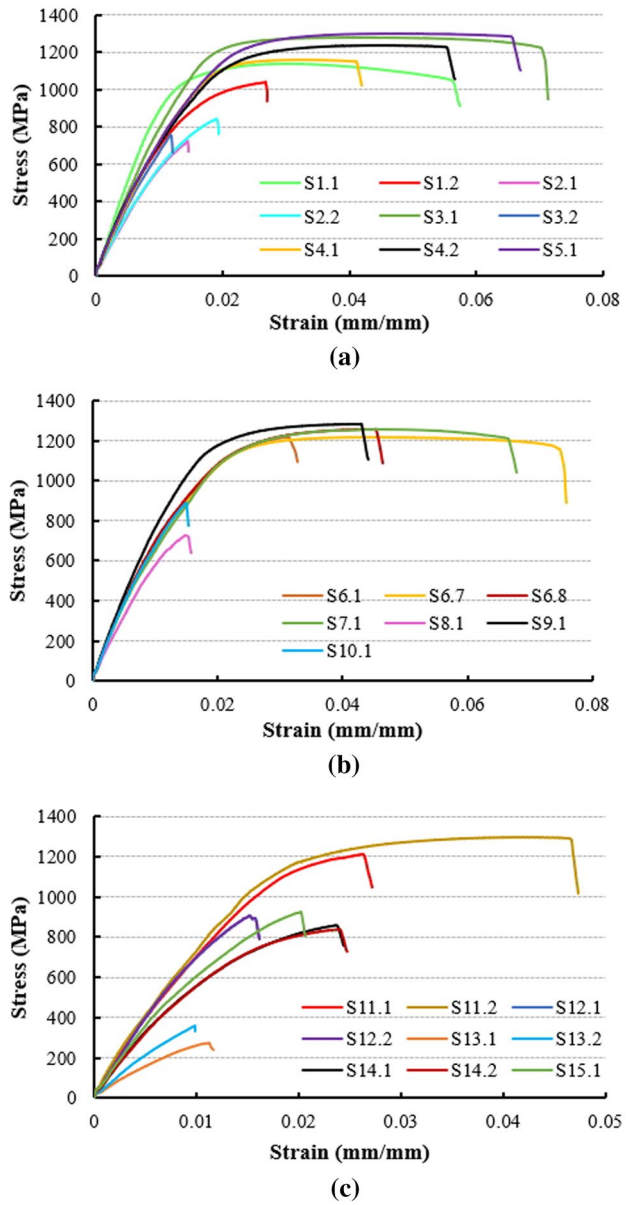

Fig. 5 Stress-strain curves of the samples

$$1250 \geq C \geq 500$$

$$90 \geq D \geq 0$$

The side constraints in Eq. (7) include limit values of the process parameters given in Table 2. Since there is no explicit mathematical expression relating the process parameters to the tensile strength, the mathematical model obtained using the RSM in this study was replaced into the optimisation problem as the objective function. Although there are several optimisation methods to solve the problem defined in Eq. (7), the PSO and GA were utilised and compared in this study. The PSO has less computational cost and ease of implementation to various real-world problems. More detailed information can be found in [28].

3.3 Optimisation results

The reduced quadratic model given in Eq. 6 was replaced as the objective function in Eq. (7), and the optimisation problem was solved using the PSO. Since a PSO algorithm has a random nature to generate new values for variables, three separate runs were carried out to ensure the convergence to an optimum value. The PSO algorithm finds optimum values for the laser power (A), layer thickness (B), scan speed (C), and build orientation (D) as 100, 39, 719, 0, respectively. The objective function yields 1342.99 MPa for the maximum tensile strength value, corresponding to the optimum process parameters.

Since most similar studies in the literature mainly utilise the GA to determine the optimum process parameters, the same model in Eq. (6) was used in the GA as a fitness function along with the side constraints defined in Eq. (7). The number of iterations needed to reach an optimum value is depicted in Fig. 6 for both the PSO and GA.

The confirmatory experiments have been conducted using the optimum values of the process parameters obtained from the optimisation run. Identically similar three samples were tested, and the mean value of these tests was taken into account. The comparison has been made between the experimentally obtained tensile strength value and the optimisation results, and reported in Table 5.

The optimum results are in good agreement with the experimental observation since the difference is less than 2%. The effect of the process parameters on the tensile strength was investigated using the response function given in Eq. (6), and the results are graphically shown as response plots in Fig. 7. The interaction of the laser power with other process parameters is given in Fig. 7a–c. As seen in Fig. 7a, the tensile strength decreases for a fixed value of the laser power as the layer thickness increases. Figure 7b shows the interaction between laser power and scan speed. A higher tensile strength was observed for a higher value of laser power, while the increase of scan speed lowers the tensile strength value beyond the optimum scan speed value (nearly 700 mm/s). It can be seen from Fig. 7c that the structure orientation angle has little effect on the tensile strength. Especially with the increased laser power, its impact on tensile strength becomes very insignificant since the laser power dominates the response value.

The response surface plots are given in Fig. 7d–f to observe the interaction of other process parameters. As seen in Fig. 7d and e, the interaction behaviour of the layer thickness with both the scan speed and build orientation angle is not linear. Higher tensile strength values can be achieved by

Table 4 Analysis of variance for the response surface model of the tensile strength

Source	DF	Adj SS	Adj MS	F-Value	*P*-value	Remarks
Model	14	1,686,220	120,444	52.45	0.000	Significant
Linear	4	992,034	248,008	107.99	0.000	Significant
Laser power (A)	1	151,170	151,170	65.83	0.000	Significant
Layer thickness (B)	1	102,630	102,630	44.69	0.000	Significant
Scan speed (C)	1	381,634	381,634	166.18	0.000	Significant
Build orientation (D)	1	4330	4330	1.89	0.195	Non-Significant
Square	4	218,375	54,594	23.77	0.000	Significant
A^2	1	8343	8343	3.63	0.081	Non-Significant
B^2	1	15,620	15,620	6.80	0.023	Significant
C^2	1	43,202	43,202	18.81	0.001	Significant
D^2	1	8837	8837	3.85	0.073	Non-Significant
2-Way Interaction	6	278,411	46,402	20.21	0.000	Significant
A*B	1	41,452	41,452	18.05	0.001	Significant
A*C	1	74,493	74,493	32.44	0.000	Significant
A*D	1	49	49	0.02	0.887	Non-Significant
B*C	1	77,679	77,679	33.83	0.000	Significant
B*D	1	4818	4818	2.10	0.173	Non-Significant
C*D	1	3193	3193	1.39	0.261	Non-Significant
Error	12	27,558	2296			
Lack-of-fit	7	23,652	3379	4.33	0.063	Non-Significant
Pure error	5	3906	781			
Total	26	1,713,778				

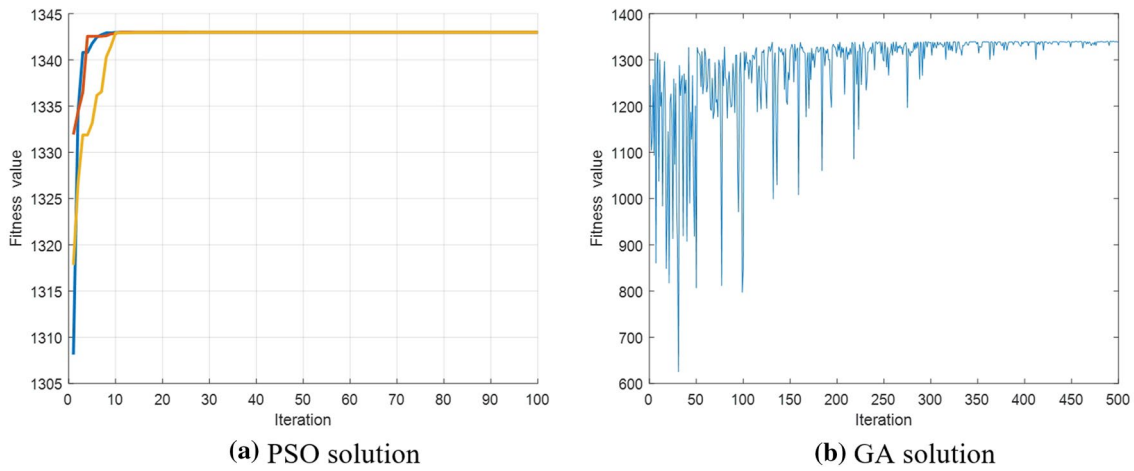

(a) PSO solution **(b)** GA solution

Fig. 6 The number of iterations both the PSO (**a**) and GA (**b**) solutions

Table 5 Validation of the PSO and GA results

	Laser power [W]	Layer thickness [μm]	Scan speed [mm/s]	Build orientation (Degree)	Optimised tensile strength (MPa)	Experimental tensile strength (MPa)
PSO	100.00	39.56	719.00	0	1342.99	1365.35
GA	99.99	39.632	713.51	0	1342.97	

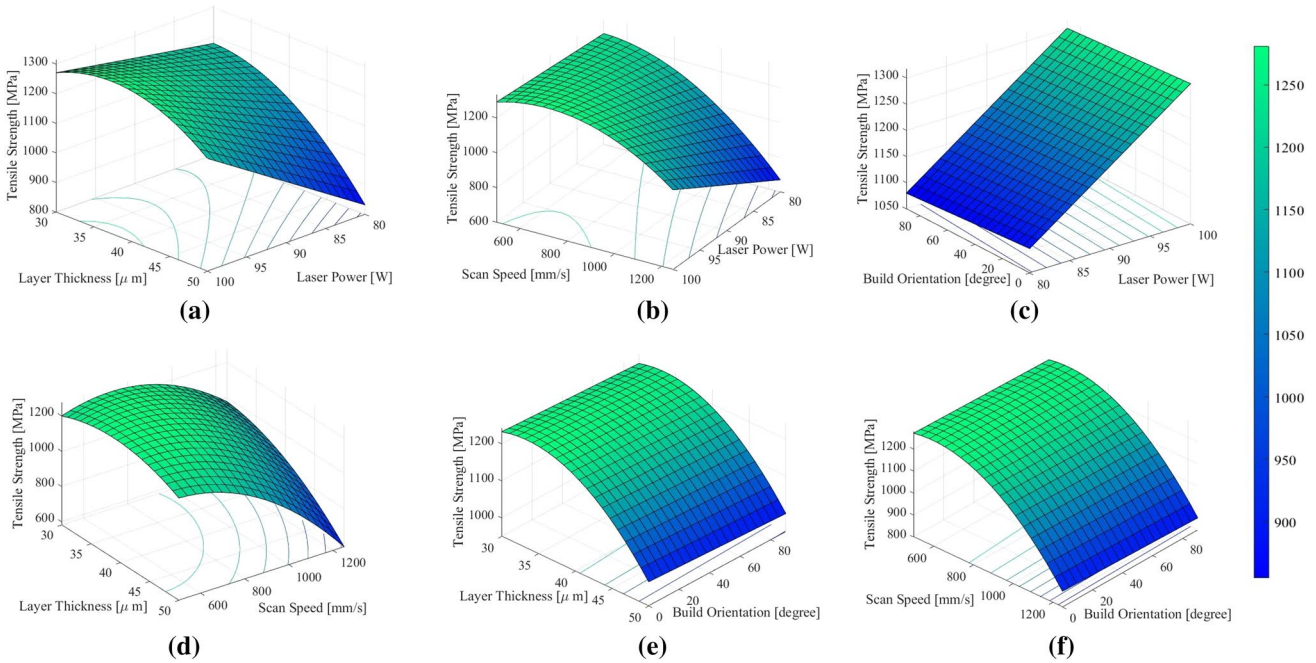

Fig. 7 Response surface plot for the interaction of laser power with the rest of the parameters **a** layer thickness, **b** scan speed, **c** build orientation and the interaction effect of **d** layer thickness with scan speed, **e** layer thickness with build orientation, and **f** scan speed with build orientation

adjusting the scan speed and layer thickness to some points near the optimum values determined by the PSO process. As seen from Fig. 7e, the interaction behaviour of the layer thickness and build orientation angle is almost linear for lower tensile strength values. In contrast, it becomes nonlinear with increased tensile strength values. Similar behaviour was observed for the scan speed and build orientation, as shown in Fig. 7f. As can be deduced from the reduced response function in Eq. 6, the build orientation is inversely proportional to the scan speed for lower tensile strength values. However, their interaction becomes nonlinear for higher values of the tensile strength.

3.4 Density measurement

Optical microscope surface images of the samples produced using different parameters are given in Fig. 8. Density was calculated by measuring black areas on the surface with ImageJ software. It was determined that the sample with the lowest density was S13.2(80-50-1250-0) in Table 3, and the density ratio in the other samples was above 98%. In this study, the density values were determined considering the cross-sectional structures examined, and the effects on mechanical behaviour were observed. It can be included in the optimization algorithm by considering the density values during the optimization process.

The surface images of samples S7.1(90-30-875-45), S13.1(80-50-1250-90) and S13.2(80-50-1250-0) are given in Fig. 9. It was observed that unmelted Ti6Al4V powders remained in the voids on the surface of the low density S13.1(80-50-1250-90) and S13.2(80-50-1250-0) samples, and pore formation [29] due to lack of fusion occurred. Low-density internal structures were obtained, as shown in Fig. 8h, because of the effect of higher scanning speed and low laser power [30]. On the other hand, an internal structure with lesser voids was obtained with the effect of laser power for a similar scanning speed.

4 Discussion

This study aims to determine the optimal processing conditions for the SLM to have the maximum tensile strength. Several methods can be utilised to find the optimum process parameters for additive manufacturing, among which the Taguchi Method is widely accepted [31, 32]. However, as outlined in the related studies [33], for nonlinear responses, other approaches such as the response surface method with a quadratic model or the artificial neural network perform better than the Taguchi method.

In this regard, rather than evaluating limited information obtained from the statistical analysis of the experiments, an optimisation method can be utilised to find the optimum process parameters. On the other hand, there is no explicit mathematical expression relating these process parameters to the tensile strength. Therefore, the RSM was used to obtain a meta-model for the implicit objective function in the

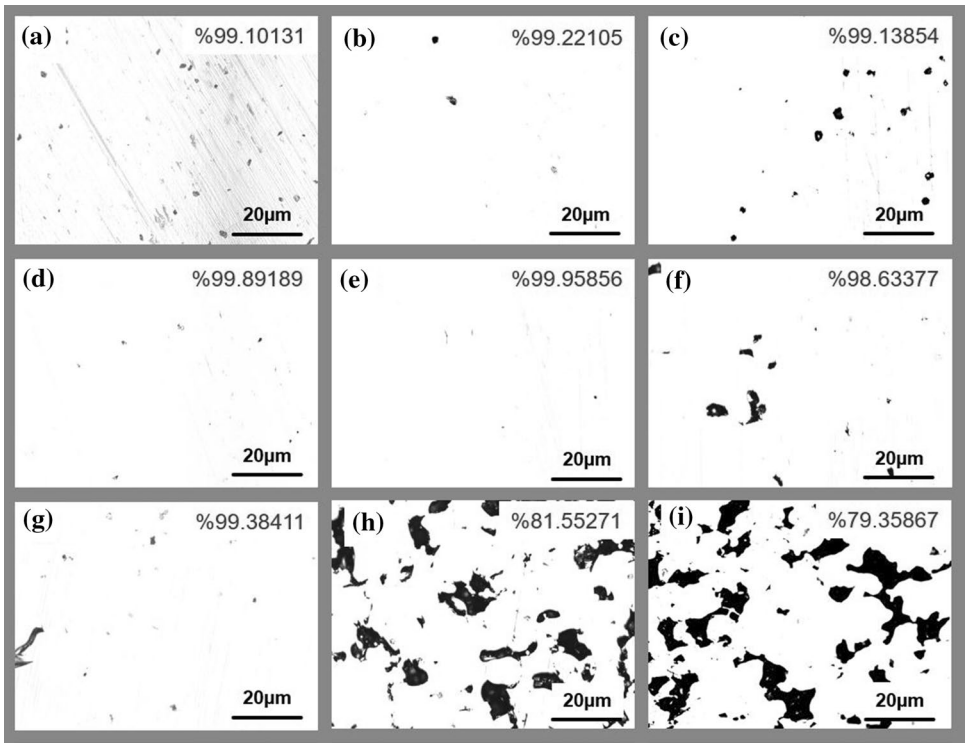

Fig. 8 Surface images of **a** S2.1, **b** S3.1, **c** S4.1, **d** S7.1, **e** S6.1, **f** S10.1, **g** S12.1, **h** S13.1, **i** S13.2 samples obtained from optical microscope

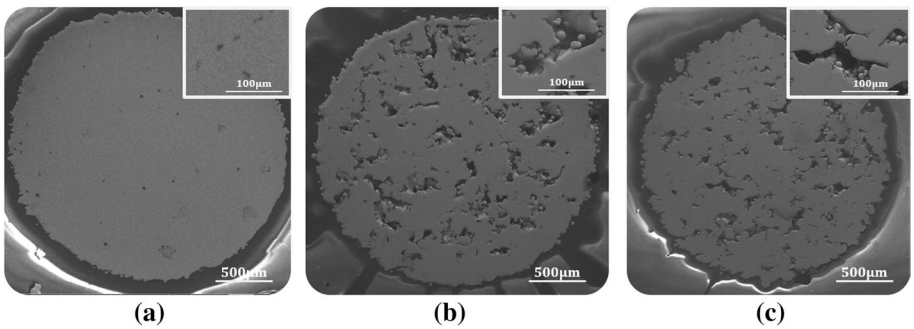

Fig. 9 SEM surface images of the samples **a** S7.1, **b** S13.1, **c** S13.2

optimisation formulation. This approach enables us to predict the optimum process parameters to maximise the tensile strength without conducting an excessive number of experiments. Moreover, the mathematical model can also predict tensile strength corresponding to the parameter values that are not tested. To obtain optimum process parameters, the GA is generally used along with a meta-model that is created for the objective function. However, the PSO algorithm and the GA were both employed in this study to get the optimum values for the selected processing parameters. Although both approaches have resulted in almost the same optimum values, the PSO reached the optimum values fewer iterations, as shown in Fig. 6.

In the SLM process, the change of temperature and cooling rate occurs very quickly [34]. This situation directly affects the mechanical properties of the product to be obtained. Therefore, the stability of the melt pool is of great importance. For example, increasing the speed will decrease strength due to LOF, and increase porosity [35], while low speed will result in less stable melt pools and coarser microstructure. In our study, the samples obtained in productions S2.1(100-50-1250-90), S2.2(100-50-1250-0) and S8.1(90-40-1250-45) confirm this situation. In addition, there is an additional effect of low laser power in productions numbered as S13.1(80-50-1250-90), S13.2(80-50-1250-0), S14.1(80-30-1250-90) and S14.2(80-30-1250-0). Significantly, the very low strengths obtained in production S13.1(80-50-1250-90) and S13.2(80-50-1250-0) show that the fusion has failed (Fig. 8). Charles et al. [36] associated this with the hydrodynamic instability of the melt, which is controlled by the Marangoni effect due to its low energy density.

As seen in Fig. 5, although the samples were manufactured from the same material (Ti6Al4V), their mechanical

behaviours are different. The maximum tensile strength of the samples varies between 1278.50 MPa and 282.53 MPa. In Figs. 8 and 9, cross-sectional images of some samples from which these different curves were obtained are given. It is seen that the melt pool formed by different parameters significantly changes the porosity. Another important feature of the melt pool is its depth since, for the layers to be bonded correctly, this depth must be greater than the thickness of a single layer [37]. Various studies have determined that the optimum layer thickness is 30 µm [38]. This was also confirmed in this study, except for the experiments with the number of S1.2(100-30-1250-0) and 2.2(100-50-1250-0). However, the opposite results were obtained for the experiment with the number of S3.1(100-50-500-90) and S4.1(100-30-500-90), which could be related to energy density. Since it is defined as $E = {}^{P}/_{vht}$, where E, P, v, h and t are quantity of laser energy, applied laser power (W), scan speed ($mm.s^{-1}$), hatching distance (mm) and layer thickness (mm), respectively, if the laser power and hatching distance parameters are assumed to be constant, the tensile strength of the samples obtained from this production decreased as a result of the higher energy density in the S4.1(100-30-500-90) production. Jiang et al. [39] reported that a large temperature gradient would occur if the energy density is higher than necessary. Thus, internal structural defects may occur, which may cause stress concentration such as residual stress, pores and interlaminar cracks, which will reduce the tensile strength. In addition, it should be noted that samples S1.1(100-30-1250-90), S1.2(100-30-1250-0), S2.1(100-50-1250-90) and S2.2(100-50-1250-0) were manufactured in different orientation angles than samples S3.1(100-50-500-90), S3.2(100-50-500-0) and S4.1(100-30-500-90), S4.2(100-30-500-0).

For a more detailed examination, the combined effect of all input parameters should be taken into account to determine their best combination, considering the interpolated values. According to the results of the current study, the system should be operated at the laser power of 100 W in order to obtain the maximum tensile strength. As discussed previousy, scan speed also has a considerable effect on the porosity level, which strongly affects the mechanical properties of the end product. For this reason, its value was determined by employing an optimisation algorithm in which the tensile strength was defined as the objective function. The optimum value for the scan speed was determined as 719 mm/s. In previous studies, the optimum scanning speed was reported in the range of 600-800 mm/s [35]. Since the optimum value of the laser power was found to be at the highest limit as previous studies [40], future studies may be designed by fixing it at 100 W and intensely focusing on other parameters in order to achieve a higher tensile strength for the additively manufactured part. Processes operating at the maximum laser power value with the high energy density enable melting, and adhesion between layers becomes more powerful. In this case, pore formation due to lack of fusion is minimised, and the possibility of damage at low stresses is reduced [37]. The building orientation directly effects mechanical properties [38] but when interacting with other laser parameters, it does not have a significant effect on the tensile properties [41]. It was reported in the literature that the decrease of the layer thickness results in an increased residual stress [42]. Therefore, the mechanical properties of the product may be adversely affected.

On the contrary, an increase from the optimum value of layer thickness leads to higher porosity [43]. In the current study, the optimum layer thickness value was found as an intermediate value of 39 µm, which is consistent with the aforementioned remarks. According to the microstructure analysis in the literature, it has been reported that the pores in the structure are the initial point for microcracks [29]. The pores in the structures are usually reduced by post-processing. It has been reported that heat treatments are insufficient to reduce the pore density, but the Hot Isostatic Pressing (HIP) method has positive effects [44].

5 Conclusions

The influence of specific process parameters on the tensile strength of the additively manufactured part has been investigated by utilising both experimental and numerical approach. The results have shown that scan speed is the most effective parameter on the mechanical properties of the additively manufactured part while the orientation angle is the least, deduced from the optimisation study carried out in this study. The optimum process parameters were determined by utilising both the PSO and GA, for which a meta-model was constructed to be used in place of the implicit objective function defined. It has been shown that the PSO outperforms the GA in reaching the optimum process parameters with less iteration. The optimum results were also verified with the experiment conducted at the optimum process parameters. The method used in this study has provided a useful numerical approach to determine the optimum operating conditions for the SLM. Thus, a significant saving can be obtained in terms of time and cost without the need of trial-and-error for the costly experiments.

Supplementary Information The online version contains supplementary material available at https://doi.org/10.1007/s12540-022-01205-9.

Acknowledgements This study is supported by the Scientific and Technological Research Council of Turkey (TUBITAK) under the project code 218M425. We would like to thank TÜBİTAK for their contributions.

Declarations

Conflict of interest The authors declared no potential conficts of interest with respect to the research, authorship, and/or publication of this article.

References

1. J. Ni, F. Liu, G. Yang, G.-H. Lee, S.-M. Chung, I.-S. Lee, C. Chen, J. Mater. Res. Technol. **14**, 2322 (2021)
2. H.M. Hamza, K.M. Deen, W. Haider, Mater. Sci. Eng. C **113**, 110980 (2020)
3. B. Song, S. Dong, H. Liao, C. Coddet, Int. J. Adv. Manuf. Technol. **61**, 967 (2012)
4. A.B. Baldissera, P. Pavez, P.A.P. Wendhausen, C.H. Ahrens, J.M. Mascheroni, IEEE Trans. Magn. **53**, 1 (2017)
5. R. Rashid, S.H. Masood, D. Ruan, S. Palanisamy, R.A.R. Rashid, J. Elambasseril, Addit. Manuf. **22**, 426–439 (2018)
6. R. Olaf, E. Claus, Wissenschaftliche Gesellschaft fur Lasertechnik. Lasertechnik **3**, 227–232 (2005)
7. H. Gong, K. Rafi, H. Gu, T. Starr, B. Stucker, Addit. Manuf. **1–4**, 87 (2014)
8. A.M. Aboutaleb, M.J. Mahtabi, M.A. Tschopp, L. Bian, J. Manuf. Proc. **38**, 432 (2019)
9. M. Simonelli, Y.Y. Tse, C. Tuck, Mater. Sci. Eng. A **616**, 1 (2014)
10. J.M. Chacón, M.A. Caminero, E. García-Plaza, P.J. Núñez, Mater. Design **124**, 143 (2017)
11. J. Li, J. Hu, L. Cao, S. Wang, H. Liu, Q. Zhou, J. Manuf. Proc. **68**, 198 (2021)
12. J. Han, J. Yang, H. Yu, J. Yin, M. Gao, Z. Wang, X. Zeng, Rapid Prototyp. J. **23**, 217 (2017)
13. A. Pawlak, P.E. Szymczyk, T. Kurzynowski, E. Chlebus, Rapid Prototyp. J. **26**, 249 (2019)
14. Z. Li, I. Kucukkoc, D.Z. Zhang, F. Liu, RPJ **24**, 150 (2018)
15. F. Ma, H. Zhang, K.K.B. Hon, Q. Gong, J. Clean. Prod. **199**, 529 (2018)
16. Y.M. Arısoy, L.E. Criales, T. Özel, B. Lane, S. Moylan, A. Donmez, Int. J. Adv. Manuf. Technol. **90**, 1393 (2017)
17. D.S. Nguyen, H.S. Park, C.M. Lee, J. Manuf. Proc. **55**, 230 (2020)
18. F.D. Wihartiko, H. Wijayanti, F. Virgantari, IOP Conf. Ser. Mater. Sci. Eng. **332**, 12020 (2018)
19. S.M. Almufti, A.Y. Zebari, H.K. Omer, J. Adv. Comput. Sci. Technol. **8**, 40 (2019)
20. J. Qin, Y. Liu, R. Grosvenor, F. Lacan, Z. Jiang, J. Clean. Prod. **245**, 118702 (2020)
21. S. Negi, S. Dhiman, R.K. Sharma, Arab. J. Sci. Eng. **39**, 9161 (2014)
22. N. Read, W. Wang, K. Essa, M.M. Attallah, Mater. Design **65**, 417 (2015)
23. D.C. Montgomery, Design and Analysis of Experiments, 6th Edn. (John Wiley & Sons, New York, 2007)
24. ASTM E8/E8M-13a, Standard test methods for tension testing of metallic materials (ASTM International, West Conshohocken, 2013)
25. M.X. Gan, C.H. Wong, J. Mater. Proces. Technol. **238**, 474 (2016)
26. Z. Ye, J. Zhu, Q. Li, B. Mo, B. Lei, Y. Li, C. Wang, C. Huang, Micro Reliab. **88–90**, 1151 (2018)
27. D. Wang, D. Tan, L. Liu, Soft. Comput. **22**, 387 (2018)
28. K. Kalita, I. Shivakoti, R.K. Ghadai, Mater. Manuf. Process. **32**, 1101 (2017)
29. A.T. Şensoy, I. Kaymaz, Ü. Ertaş, Swarm Evol. Comput. **53**, 100645 (2020)
30. P.-H. Li, W.-G. Guo, W.-D. Huang, Y. Su, X. Lin, K.-B. Yuan, Mater. Sci. Eng. A **647**, 34 (2015)
31. M. Tang, L. Zhang, N. Zhang, Mater. Sci. Eng. A **814**, 141187 (2021)
32. J. Sun, Y. Yang, D. Wang, Opt. Laser Technol. **49**, 118 (2013)
33. B. Yang, Y. Lai, X. Yue, D. Wang, Y. Zhao, Scanning **2020**, 9176509 (2020)
34. B. Fotovvati, M. Balasubramanian, E. Asadi, Coatings **10**, 1104 (2020)
35. G. Kasperovich, J. Haubrich, J. Gussone, G. Requena, Mater. Design **105**, 160 (2016)
36. A.K. Singla, M. Banerjee, A. Sharma, J. Singh, A. Bansal, M.K. Gupta, N. Khanna, A.S. Shahi, D.K. Goyal, J. Manuf. Process. **64**, 161 (2021)
37. A. Charles, A. Elkaseer, L. Thijs, S.G. Scholz, Appl. Sci. **10**, 7 (2020)
38. T. Vilaro, C. Colin, J.D. Bartout, Metall. Mater. Trans. A **42**, 3190 (2011)
39. J.T. Oliveira de Menezes, E.M. Castrodeza, R. Casati, Mater. Sci. Eng. A **766**, 138392 (2019)
40. Q. Jiang, S. Li, C. Zhou, B. Zhang, Y. Zhang, Opt. Laser Technol. **144**, 107391 (2021)
41. A.H. Maamoun, Y.F. Xue, M.A. Elbestawi, S.C. Veldhuis, Materials **12**, 12 (2019)
42. S. Pal, N. Gubeljak, R. Hudak, G. Lojen, V. Rajtukova, J. Predan, V. Kokol, I. Drstvensek, Mater. Sci. Eng. A **743**, 637 (2019)
43. C. Qiu, C. Panwisawas, M. Ward, H.C. Basoalto, J.W. Brooks, M.M. Attallah, Acta Mater. **96**, 72 (2015)
44. L. van Belle, J.-C. Boyer, G. Vansteenkiste, Key Eng. Mater. **554-557**, 1828 (2013)
45. S. Leuders, M. Thöne, A. Riemer, T. Niendorf, T. Tröster, H.A. Richard, H.J. Maier, Int. J. Fatigue **48**, 300 (2013)